13

Modification of transverse shear stiffness of shell element

In order to improve the performance of a four-node shell element in bending, the transverse shear energy and stiffness must be treated in a special way. The two main problems are the transverse shear locking (TSL) and the poor performance of very thin elements. These problems also appear for beams, which are simpler and more suitable for analytical studies.

13.1 Treatment of transverse shear stiffness of beams

To identify the problems related to the transverse shear, it suffices to consider the linear kinematics and small rotations of the Timoshenko beam.

Timoshenko beam equations. For the Timoshenko beam, the membrane, transverse shear, and bending strain components are as follows:

$$\varepsilon_{xx} = u_{x,x}, \qquad 2\varepsilon_{zx} = w_{,x} - \theta \doteq \gamma, \qquad \kappa_{xx} = -\theta_{,x}, \tag{13.1}$$

where u is a tangent displacement, w is the normal displacement, and θ is the rotation angle of the middle line of the beam. The strain energy is

$$\mathcal{W} \doteq \int_0^L (\mathcal{W}_\varepsilon + \mathcal{W}_\gamma + \mathcal{W}_\kappa)\,\mathrm{d}x, \tag{13.2}$$

where

$$\mathcal{W}_\varepsilon \doteq \frac{1}{2} EA\,\varepsilon_{xx}^2, \qquad \mathcal{W}_\gamma \doteq k\,2GA\,\varepsilon_{zx}^2 = \frac{1}{2} k\,GA\,\gamma^2, \qquad \mathcal{W}_\kappa \doteq \frac{1}{2} EI\,\kappa_{xx}^2.$$

Besides, $k = 5/6$ is the shear correction coefficient and L is the beam length. For a rectangular cross-section of the beam of height h and width b, the area is $A = bh$, and the moment of inertia is $I = bh^3/12$.

Transverse shear strain for large rotation beam. Consider a straight (not curved) beam in the 13-plane (XZ-plane). The transverse shear strain of a beam in the ortho-normal basis $\{\mathbf{t}_k\}$ $(k = 1, 3)$ is as follows:

$$\varepsilon_{13} = \tfrac{1}{2}\mathbf{x}_{0,x} \cdot \mathbf{a}_3. \tag{13.3}$$

The form of this strain is identical for the Green strain and the symmetric right stretch strain. The rotation tensor is

$$\mathbf{Q} = c\,(\mathbf{t}_1 \otimes \mathbf{t}_1 + \mathbf{t}_3 \otimes \mathbf{t}_3) + s\,(\mathbf{t}_3 \otimes \mathbf{t}_1 - \mathbf{t}_1 \otimes \mathbf{t}_3), \quad s \doteq \sin\theta, \quad c \doteq \cos\theta, \tag{13.4}$$

where θ is the rotation angle about the axis $\mathbf{t}_2$. Then $\mathbf{a}_3 \doteq \mathbf{Q}\,\mathbf{t}_3 = c\,\mathbf{t}_3 - s\,\mathbf{t}_1$. Besides, $\mathbf{x}_{0,x} = (\mathbf{y}_0 + \mathbf{u}_0)_{,x} = \mathbf{t}_\alpha + \mathbf{u}_{,x}$, where $\mathbf{u} = u\mathbf{t}_1 + w\mathbf{t}_3$. For a straight beam, $\mathbf{t}_{1,x} = \mathbf{t}_{3,x} = \mathbf{0}$, and eq. (13.3) becomes

$$2\varepsilon_{13} = \mathbf{x}_{0,x} \cdot \mathbf{a}_3 = -s - u_{,x}\,s + w_{,x}\,c. \tag{13.5}$$

For small rotations, $\theta \approx 0$, we have $s \approx \theta$ and $c \approx 1$ and neglecting the second order term $u_{,x}\,\theta$, we obtain the linearized transverse shear strain of eq. (13.1).

13.1.1 Reduced integration of transverse shear energy

Transverse shear locking. The transverse shear locking (TSL) is a pathological phenomenon plaguing elements based on the Reissner hypothesis and low-order approximations. It manifests itself in two ways:

1. an artificial over-stiffening of an FE model is observed for coarse meshes. The solution is too small, compared to the analytical solution, see Fig. 13.1. In other words, the solution is "locked".

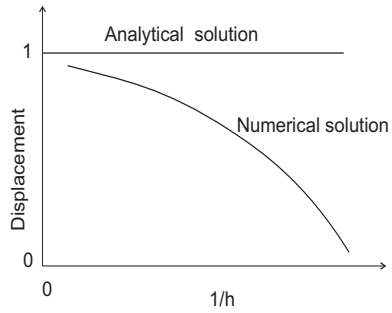

Fig. 13.1 Locking of numerical solution.

2. The rate of the mesh convergence deteriorates and a much denser mesh is necessary to obtain an accurate solution. In the mesh limit, however, the solution is correct.

The TSL is caused by two factors:

1. improper approximation of the transverse shear strain, due to non-matching approximations of particular terms and
2. high values of the (transverse shear stiffness/bending stiffness) ratio for very small thickness h. This ratio is proportional to $12/h^2$, so the thickness is a critical parameter.

We stress that the TSL is not caused by finite computer representations and arithmetic and its presence can be shown in an analytical way, e.g. considering pure bending of a beam element. The first papers on the subject were [226, 227].

Transverse shear locking of two-node beam. Assume that the element's center is located at $x = 0$, see Fig. 13.2. Then $x = (l/2)\,\xi$, where $\xi \in [-1, +1]$, l is the element's length, and we differentiate as follows:

$$(\,\cdot\,)_{,x} = (\,\cdot\,)_{,\xi} \left(\frac{\mathrm{d}x}{\mathrm{d}\xi}\right)^{-1} = \frac{2}{l}\,(\,\cdot\,)_{,\xi}. \tag{13.6}$$

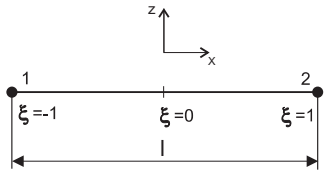

Fig. 13.2 Two-node beam element.

To derive a two-node beam element, we use the approximations

$$w(\xi) = \sum_{I=1}^{2} N_I(\xi)\, w_I, \qquad \theta(\xi) = \sum_{I=1}^{2} N_I(\xi)\, \theta_I, \tag{13.7}$$

where $(\,\cdot\,)_I$ designates the nodal values and the linear shape functions are

$$N_1(\xi) \doteq \frac{1}{2}(\xi - 1), \qquad N_2(\xi) \doteq \frac{1}{2}(\xi + 1). \tag{13.8}$$

For these approximations, the components of $\varepsilon_{xz}(\xi)$ of eq. (13.1) are as follows:

$$\theta(\xi) = \tfrac{1}{2}(1-\xi)\,\theta_1 + \tfrac{1}{2}(1+\xi)\,\theta_2, \qquad w_{,x}(\xi) = \frac{1}{L}(w_2 - w_1), \tag{13.9}$$

i.e. $\theta(\xi)$ is a linear function, while $w_{,x}(\xi)$ is a constant function. We see that approximations of these two components do not match up, which has negative consequences.

For pure cylindrical bending of the two-node beam element, see Fig. 13.3, the nodal displacements $w_2 = w_1$ and the nodal rotations $\theta_1 = -\theta$ and $\theta_2 = \theta$. Hence, $\theta(\xi) = \xi\,\theta$ and $w_{,x} = 0$, so we obtain

$$2\varepsilon_{xz}(\xi) = \xi\,\theta, \tag{13.10}$$

which is a linear function of ξ. The analytical value of $\varepsilon_{zx}(\xi)$ for pure bending is zero and is obtained from the above formula only at one point, $\xi = 0$, i.e. at the element's center. This observation is exploited by the reduced integration technique described in the sequel.

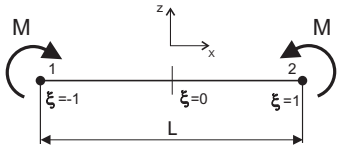

Fig. 13.3 Pure cylindrical bending of two-node beam element.

Remark on transverse shear locking of three-node beam element. Note that the TSL also appears for the three-node beam element based on quadratic shape functions. However, the TSL does not appear for pure bending, but for the transverse loads shown in Fig. 13.4. Two points, $\xi = \pm 1/\sqrt{3}$, at which the approximated $\varepsilon_{zx}(\xi)$ yields analytical values can be found as a solution of a quadratic equation, see [94].

Reduced integration (SRI and URI) of transverse shear energy. To avoid the TSL, we can use the numerical Gauss integration based on the points at which ε_{zx} is correct.

For instance, for a two-node beam, we may use the one-point integration rule using the point $\xi = 0$, while, for the three-node beam, we may

Fig. 13.4 Bending of three-node beam element by force P and distributed load q.

use the two-point integration rule exploiting the points, $\xi = \pm 1/\sqrt{3}$. Fortunately, in both cases, the under-integration does not yield spurious zero eigenvalues of the tangent matrix.

Two forms of the reduced integration are in use. Within the Selective Reduced Integration (SRI) technique, only the transverse shear strain energy is under-integrated. However, for a two-node beam, we can uniformly under-integrate all terms of the strain energy and the element's rank still remains correct. Such a technique is called the Uniform Reduced Integration (URI). If the reduced integration technique yields spurious zero eigenvalues of the tangent matrix, then it must be additionally stabilized.

The SRI technique works very well for beams; the accuracy of the SRI integration and the full integration is compared in [103], Tables I and II, for the example of a cantilever beam loaded by a transverse force.

Why poor approximation of transverse shear strain locks the solution. Consider only the transverse shear and bending strain components in the beam strain energy of eq. (13.2), which can be rewritten as follows:

$$2\mathcal{W}/EI = \int_{-l/2}^{l/2} \left(\kappa_{xx}^2 + \alpha\, \varepsilon_{xz}^2\right)\, \mathrm{d}x, \qquad \alpha \doteq \frac{k2GA}{EI}. \tag{13.11}$$

For a rectangular cross-section, when $A = bh$ and $I = bh^3/12$,

$$\alpha = \frac{24kG}{Eh^2} = \frac{12k}{(1+\nu)}\frac{1}{h^2}.$$

If the thickness $h \to 0$, then $\alpha \to \infty$, and the component $\alpha\, \varepsilon_{xz}^2 = \alpha\, (\varepsilon_{xz} - 0)^2$ can be interpreted as the penalty term enforcing the condition $\varepsilon_{xz} = 0$. This condition is physically correct for $h \to 0$.

The problem appears when ε_{xz} is not properly approximated within an element because then, not $\varepsilon_{xz} = 0$, but some other condition is

enforced. This can be shown for pure bending, for which $2\varepsilon_{xz}(\xi) = \xi\,\theta$, see eq. (13.10). Then, the transverse shear term is

$$\int_{-l/2}^{l/2} \varepsilon_{xz}^2 \,\mathrm{d}x = \frac{l}{2}\int_{-1}^{1} \varepsilon_{xz}^2 \,\mathrm{d}\xi = \frac{l}{12}\,\theta^2, \tag{13.12}$$

and, eq. (13.11) becomes

$$2\mathcal{W}/EI = \int_{-l/2}^{l/2} \kappa_{xx}^2 \,\mathrm{d}x + \alpha\,\frac{l}{12}\,(\theta - 0)^2. \tag{13.13}$$

We see that for $\alpha \to \infty$, the condition $\theta = 0$ is enforced, which is non-physical and causes an over-stiffened response (locking) of the two-node beam element.

13.1.2 Residual Bending Flexibility (RBF) correction

Introduction. Low-order elements, such as a two-node Timoshenko beam element and a four-node Reissner shell element, seriously lock for the sinusoidal bending shown in Fig. 13.5a, because this form of deformation cannot be properly represented by linear (or bilinear) shape functions. To remedy this problem, we can use the corrected value of the transverse shear stiffness defined as follows:

$$(GA)^* \doteq c_{\mathrm{RBF}}\,GA, \tag{13.14}$$

where c_{RBF} is a scalar coefficient determined by the method of the Residual Bending Flexibility (RBF), which is described below. Note that

1. the RBF correction does not affect the cylindrical (pure) bending shown in Fig. 13.5b, for which the transverse shear strain is zero. This type of bending is improved by the reduced integration of the transverse shear energy or proper sampling of the transverse shear strain.
2. The RBF correction is beneficial for extremely thin elements when the elemental aspect ratio (l/h) is very large. For this case, we also can use the scaling down of [103], discussed in the sequel.

The RBF correction was proposed for beams in [198] and adapted for shells in [138].

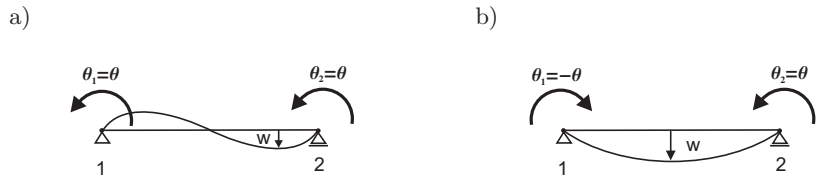

Fig. 13.5 Bending of beam: a) Sinusoidal bending. b) Cylindrical (pure) bending.

RBF correction for beam. For two-node Timoshenko beams, the RBF correction amounts to using, in computations, the corrected value of a transverse shear stiffness

$$(GA)^* = \left(\frac{1}{GA} + \frac{l^2}{12EI} \right)^{-1}, \tag{13.15}$$

where the second term, $l^2/(12EI)$, is designated as the *residual bending flexibility* (RBF) and l is the element's length. For a rectangular cross-section when $A = bh$ and $I = bh^3/12$, we can define the corrected shear modulus

$$G^* \doteq \frac{(GA)^*}{A} = \frac{h^2 EG}{h^2 E + l^2 G} = \left(\frac{1}{G} + \frac{l^2}{h^2 E} \right)^{-1}. \tag{13.16}$$

The RBF term does not vanish since $l \neq 0$, and dominates for $l/h > \sqrt{E/G} = \sqrt{2(1+\nu)}$. If the RBF term strongly dominates, i.e. when $l/h \gg \sqrt{E/G}$, then we can neglect $1/(GA)$ in eq. (13.15), which yields

$$(GA)^* \approx \frac{12EI}{l^2} \qquad \text{and} \qquad G^* \approx \left(\frac{h}{l} \right)^2 E. \tag{13.17}$$

These formulas are well suited for elements of large (l/h) aspect ratios.

Derivation of the RBF correction for a beam. The derivation below is for a small strain/small rotation beam, but the obtained corrected transverse shear stiffness is subsequently tested also on non-linear problems.

We drive a two-node Discrete Kirchhoff (DK) beam element with the normal displacement approximated by a cubic polynomial

$$w(\xi) = a_0 + a_1\,\xi + a_2\,\xi^2 + a_3\,\xi^3, \qquad \xi \in [-1, +1]. \tag{13.18}$$

Using the boundary conditions: $w(-1) = w_1$, $w(+1) = w_2$, $w_{,\xi}(-1) = (w_{,\xi})_1$, and $w_{,\xi}(+1) = (w_{,\xi})_2$, we can determine the coefficients a_i $(i = 0, 1, 2, 3)$ and rewrite eq. (13.18) as

$$w(\xi) = N_1(\xi)\, w_1 + N_2(\xi)\, w_2 + N_3(\xi)\, (w_{,\xi})_1 + N_4(\xi)\, (w_{,\xi})_2, \qquad (13.19)$$

where the Hermitian shape functions are

$$N_1(\xi) \doteq \frac{1}{2} - \frac{3\xi}{4} + \frac{\xi^3}{4}, \qquad N_2(\xi) \doteq \frac{1}{2} + \frac{3\xi}{4} - \frac{\xi^3}{4},$$
$$N_3(\xi) \doteq \frac{1}{4}(1 - \xi - \xi^2 + \xi^3), \quad N_4(\xi) \doteq \frac{1}{4}(-1 - \xi + \xi^2 + \xi^3), \quad (13.20)$$

see Fig. 13.6.

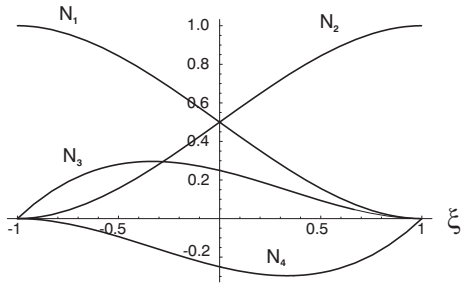

Fig. 13.6 Hermitian shape functions N_1, N_2, N_3, and N_4.

The Kirchhoff constraint, $\varepsilon_{13} = 0$, yields the relation $\theta = w_{,x}$. Applying this constraint to discrete points, namely to the boundary nodes, and using $w_{,x} = (2/l) w_{,\xi}$, we obtain $(w_{,\xi})_1 = (l/2)\,\theta_1$ and $(w_{,\xi})_2 = (l/2)\,\theta_2$. Hence, the normal displacement becomes

$$w(\xi) = N_1(\xi)\, w_1 + N_2(\xi)\, w_2 + \frac{l}{2}\left[N_3(\xi)\,\theta_1 + N_4(\xi)\,\theta_2\right], \qquad (13.21)$$

where θ_1 and θ_2 are the nodal rotations. This form of w is used in the sequel, as it conforms with the boundary conditions for the cases shown in Fig. 13.5. Note that we can separate the terms for the cylindrical and sinusoidal bending as follows:

$$\frac{l}{2}\left[N_3(\xi)\,\theta_1 + N_4(\xi)\,\theta_2\right] = \frac{l}{8}[\underbrace{(1-\xi^2)}_{\text{cylindrical}}(\theta_1 - \theta_2) + \underbrace{(-\xi+\xi^3)}_{\text{sinusoidal}}(\theta_1 + \theta_2)], \qquad (13.22)$$

and if $\theta_1 = \pm\theta_2$, then only one type of bending remains.

Let us now define components of the strain energy of the DK beam element:

1. the bending energy

$$\mathcal{W}_\kappa \doteq \frac{l}{4}\int_{-1}^{+1} EI\ \kappa^2\ \mathrm{d}\xi, \qquad \kappa = -\frac{4}{l^2} w_{,\xi\xi}, \tag{13.23}$$

   where the bending strain $\kappa = -\theta_{,x} \approx -w_{,xx}$ for the Kirchhoff constraint.
2. the transverse shear energy

$$\mathcal{W}_\gamma \doteq \frac{l}{4}\int_{-1}^{+1} GA\ \gamma^2\ \mathrm{d}\xi, \qquad \gamma = \frac{EI}{GA}\frac{2}{l}\,\kappa_{,\xi}, \tag{13.24}$$

   where the transverse shear strain $\gamma = -(EI/GA)\,\kappa_{,x}$ is recovered from the equilibrium equation $Q = -M_{,x}$, in which we used $M = EI\,\kappa$ and $Q = GA\,\gamma$.

Using these energies, we can define the ratio of the shear energy to the total energy

$$c \doteq \frac{\mathcal{W}_\gamma}{\mathcal{W}_\kappa + \mathcal{W}_\gamma}. \tag{13.25}$$

For the sinusoidal bending of Fig. 13.5b, we have $w(\xi) = \frac{l}{4}\,\xi(\xi^2 - 1)\,\theta$ and the above formulas yield

$$\mathcal{W}_\kappa = \frac{6EI}{l}\theta^2, \quad \mathcal{W}_\gamma = \frac{72(EI)^2}{GAl^3}\theta^2, \quad c_{\mathrm{RBF}} \doteq c = \frac{12EI}{12EI + GAl^2}, \tag{13.26}$$

where c_{RBF} does not depend on the rotation θ ! Note that these formulas are for the beam element based on cubic displacements (13.18), but we shall apply the coefficient c_{RBF} to the two-node Timoshenko beam element, which is based on linear displacements and rotation.

Sinusoidal bending of very slender beam. Consider the sinusoidal bending of a very slender beam element, for which $h/l \ll 1$. Then, for the DK beam element based on cubic displacements, the bending energy dominates in eq. (13.26), i.e. $\mathcal{W}_\kappa \gg \mathcal{W}_\gamma$, so

$$\mathcal{W} \doteq \mathcal{W}_\kappa + \mathcal{W}_\gamma \approx \mathcal{W}_\kappa = \frac{6EI}{l}\theta^2, \tag{13.27}$$

where $\mathcal{W}_\gamma$ is neglected. On the other hand, for a two-node Timoshenko element with linear approximations of θ and w, the sinusoidal bending yields

$$\mathcal{W} \doteq \mathcal{W}_\kappa + \mathcal{W}_\gamma = \mathcal{W}_\gamma = \frac{GA\,l}{2}\theta^2, \tag{13.28}$$

i.e. only the transverse shear energy is non-zero. These two energies are equal if $GA = 12EI/l^2$, so we define $(GA)^* \doteq 12EI/l^2$ which has the form of eq. (13.14). For this corrected transverse shear stiffness, the two-node Timoshenko element with linear approximation of w yields almost identical nodal rotations as the DK beam element based on a cubic approximation of w.

13.1.3 Scaling down of transverse shear stiffness

For extremely thin beam and shell elements, we obtain very inaccurate solutions. This is attributed to disparity between the orders of bending and shear terms, which means that, due to the finite computer precision, the bending stiffness is annihilated.

Then, either the RBF correction or the method of scaling down the transverse shear stiffness proposed in [103] can be applied. The most important difference between these two methods is that the scaling down does not pertain to any particular form of deformation, while the RBF method does.

In the method of scaling down the transverse shear stiffness, the annihilation of the bending stiffness is prevented by the following strategy:

1. We find the maximum aspect ratio of an element, $(l/h)_{\max}$, for which the accuracy is still correct. This value is determined by a numerical experiment and $10^4/16$ for beams and $10^5/8$ for plates was found in the cited work.
2. For the aspect ratios which are larger than the maximum aspect ratio, i.e. for $l/h > (l/h)_{\max}$, we scale down the transverse shear stiffness

$$(GA)^* \doteq s\ GA, \qquad s \doteq \left(\frac{h}{l}\right)^2 \left(\frac{l}{h}\right)^2_{\max}. \tag{13.29}$$

The scaling factor s is plotted in Fig. 13.7 and we see that it tends to zero for $l/h \to \infty$. Then the strain energy of a beam is

$$2\mathcal{W} = \int_{-l/2}^{l/2} \left[EI\kappa_{xx}^2 + (GA)^*\,\varepsilon_{xz}^2\right]\,\mathrm{d}x. \tag{13.30}$$

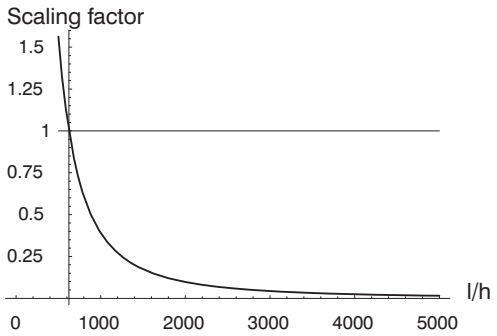

Fig. 13.7 Scaling factor for $(l/h)_{\max} = 10^4/16$.

Alternatively, we can scale down the ratio of the shear stiffness to the bending stiffness α of eq. (13.11),

$$\alpha^* \doteq s\ \alpha, \tag{13.31}$$

so the strain energy of eq. (13.11) becomes

$$2\mathcal{W}/EI = \int_{-l/2}^{l/2} \left(\kappa_{xx}^2 + \alpha^*\, \varepsilon_{xz}^2\right)\, \mathrm{d}x. \tag{13.32}$$

Both above forms of the strain energy are equivalent. Note that the above scaling down is in accord with eq. (13.27) for sinusoidal bending of a very slender beam.

Scaling down parameter s. The scaling down parameter s of eq. (13.29) can be obtained by the simple reasoning presented below. The estimation of energy components of a two-node Timoshenko beam element is as follows:

1. the bending energy

$$\mathcal{W}_\kappa \doteq \frac{1}{2}\frac{Eh^3}{12}\int_0^l \theta_{,x}^2\ \mathrm{d}x \approx \frac{1}{2}\frac{Eh^3}{12}\frac{(\theta_2-\theta_1)^2}{l}, \tag{13.33}$$

2. the shear energy

$$\begin{aligned}\mathcal{W}_\gamma &\doteq \frac{1}{2}kGh\int_0^l (w_{,x}-\theta)^2\ \mathrm{d}\xi \\ &\approx \frac{1}{2}kGh\left[\frac{(w_2-w_1)^2}{l} - 2(w_2-w_1)\,\theta_c + \theta_c^2\, l\right],\end{aligned} \tag{13.34}$$

where $\theta_c \doteq \frac{1}{2}(\theta_1+\theta_2)$ is the rotation at the element's center.

The order of the bending stiffness S_κ and the shear stiffness S_γ is as follows:

$$S_\kappa \doteq \frac{\partial \mathcal{W}_\kappa}{\partial \theta_\alpha} \sim \frac{h^3}{l}, \qquad S_\gamma \doteq \frac{\partial \mathcal{W}_\gamma}{\partial \theta_\alpha} \sim hl, \qquad \alpha = 1, 2, \tag{13.35}$$

and their ratio is

$$\frac{S_\kappa}{S_\gamma} = \left(\frac{h}{l}\right)^2. \tag{13.36}$$

We see that, for the aspect ratio $(l/h) \to \infty$, the ratio $(S_\kappa/S_\gamma) \to 0$. Because S_κ is much smaller than S_γ, the bending stiffness is annihilated due to finite computer precision. The effect of disparity between the bending and shear term is alleviated if we scale down as in eq. (13.29).

13.1.4 Numerical tests for beams

Test 1. Transverse shear locking of cantilever. One boundary of a cantilever is fixed while at the other one a vertical force $P = 1$ is applied. The data is as follows: $E = 3 \times 10^6$, $\nu = 0.3$, $L = 100$, $h = 3$, $b = 1$. The two-node Timoshenko beam element is integrated using either one- or two-point Gauss integration of the transverse shear energy.

The mesh convergence for the linear test is shown in Fig. 13.8, where the normalizing value is 4.9416×10^{-2}. We see that the element with the two-point integration converges very slowly while the element using one-point integration converges quickly. The difference is significant, as four elements with one-point integration provide better accuracy than 100 elements with two-point integration.

Test 2. Eigenvalues. Effect of the RBF correction. Two types of two-node Timoshenko beam elements are checked:

1. the element designated as "Linear" is based on linear shape functions. The bending and membrane energy is integrated using either one point at the element's center or two Gauss points, while the shear strain energy is integrated at the element center,
2. the element designated as "Allman" is based on Allman-type shape functions so the displacement vector is approximated as follows:

$$\mathbf{u}_0 = \mathbf{u}_0^L - \frac{l}{8}(1 - \xi^2)(\theta_2 - \theta_1)\,\mathbf{n}, \tag{13.37}$$

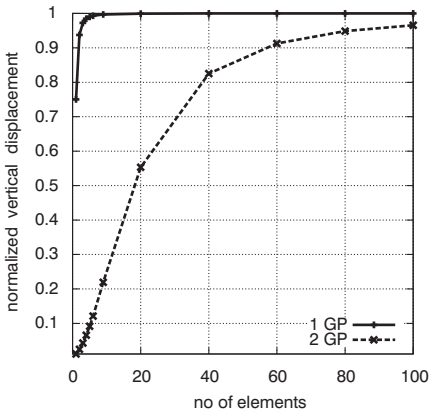

Fig. 13.8 Cantilever loaded by vertical force. Effect of integration rule for transverse shear.

where $\mathbf{u}_0^L$ is approximated by linear shape functions, θ_1, θ_2 are nodal rotations, and $\mathbf{n}$ is a vector normal to the element. (For more details on Allman shape functions, see Sect. 12.7.) The bending and membrane energy is integrated using two Gauss points, while the shear strain energy is integrated by one Gauss point, at the element's center.

We see in Table 13.1 that both elements have identical eigenvalues and the second eigenvalue, which is associated with the transverse shear, is decreased about 33 times by the RBF correction.

Table 13.1 Non-zero eigenvalues of two-node beam elements based on Green strain. $E = 10^6, \quad \nu = 0.3, \quad h = 0.1, \quad l = 1, \quad b = 1.$

Shape functions	Non-zero eigenvalues		
no transverse shear stiffness			
Linear	0.2000E+06		0.1667E+03
Allman	0.2000E+06		0.1667E+03
with transverse shear			
Linear	0.2000E+06	0.8013E+05	0.1667E+03
Allman	0.2000E+06	0.8013E+05	0.1667E+03
transverse shear with RBF correction			
Linear	0.2000E+06	0.2424E+04	0.1667E+03
Allman	0.2000E+06	0.2424E+04	0.1667E+03

Test 3. Sinusoidal bending of simply supported beam. The beam is simply supported and loaded by two end moments $M_1 = M_2 = 1$, which gener-

ate the sinusoidal bending of Fig. 13.5a. The results for the Timoshenko beam element ("Linear") with/without the RBF correction are shown in Table 13.2. We see that, for a single element, the solution obtained without the RBF correction is severely locked, but the RBF correction is a perfect remedy. Note that $h/l \in [0.0001, 0.01]$ and the coefficient c_{RBF} assumes values greatly differing from 1!

For comparison, also the solution for three-node beam element is provided. This element is based on parabolic shape functions and uses the two-point Gauss URI. The Assumed Strain (AS) method of [94] for the membrane and transverse shear strains, with two sampling points and the three-point Gauss integration yields exactly the same results.

Table 13.2 Sinusoidal bending by two-node beam element. Effect of RBF correction. $E = 2.11 \times 10^{11}$, $\nu = 0.3$, $h = 0.0002$, $l = 2$, $b = 2$.

	Rotation at node 1			
No of elements	1	2	10	100
no RBF	7.3934E-08	1.7773	2.3460	2.3694
RBF	2.3697	2.3697	2.3697	2.3697
three-node beam	2.3697	2.3697	2.3697	2.3697
h/l of element	0.0001	0.005	0.001	0.01
c_{RBF}	3.119E-08	1.247E-7	3.119E-06	3.119E-04

Test 4. Linear and non-linear cantilever beam. The data is the same as in Test 1. Two finite-rotation two-node Timoshenko beam elements, based on either "Linear" or "Allman" shape functions, and either with or without the RBF correction are used. In the linear test, the load $P = 1$, while in the nonlinear one, the initial load increment $\Delta P = 10$ and the arc-length method is used.

The mesh convergence for the linear test is shown in Fig. 13.9a, where the normalizing value is 4.9416×10^{-2}, and the exact solution is obtained, even for one element. In the non-linear test, see Fig. 13.9b, the reference solution is obtained for 10 elements for which the effect of the RBF correction vanishes. For the mesh of two elements based on "Linear" shape functions and without the RBF correction, the solution is almost exact, while the correction yields a slightly too soft solution. For the same mesh, the solutions for the element based on the "Allman" shape functions are correct only up to a certain load but for the 10-element mesh they are close to the reference solution in the whole range.

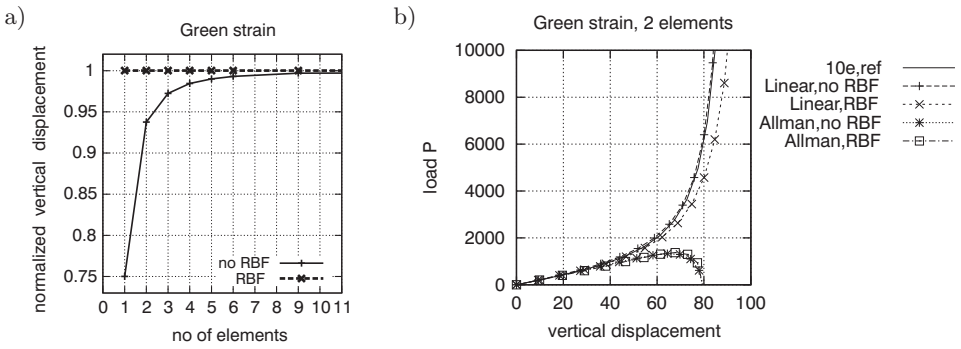

Fig. 13.9 Cantilever loaded by vertical force. Effect of the RBF correction. a) Linear test. Mesh convergence. b) Nonlinear test.

Test 5. Extremely thin cantilever beam. The purpose of this test is to compare the scaling down of the transverse shear stiffness of eq. (13.29) with the RBF correction for the extreme thinness in a linear example involving the transverse shear. The value $(l/h)_{\max} = 10^4/16$ was used for the scaling down.

One boundary of a cantilever is fixed, while at the other one, a vertical force P is applied. The data is as follows: $E = 10^6$, $\nu = 0.3$, $L = 100$, $b = 1$, the load $P = 1$. The two-node Timoshenko beam element based on one-point Gauss integration is used and 100 elements are applied. Hence, the length of a single element is $l = 1$, while the thickness is varied, $h = 10^n$, $n \in [0, -8]$.

The results are given in Table 13.3, where the normal displacement w and the rotation θ at the beam's tip are presented. We see that, for the not modified element, the accuracy is acceptable only for up to $(l/h) = 10^{-4}$, while for the RBF correction and the scaling of eq. (13.29), the accuracy is good even for $(l/h) = 10^{-8}$. We note a 5% error appearing for both these methods for $h = 10^{-5}$.

13.1.5 Curvature correction

Two-node beam elements are typically defined by node positions and are straight. If they are used for curved beams or arches and coarse meshes, then the accuracy can be improved if we account for curvature. The curvature can be defined by specifying either normal vectors at nodes or the height of the arch, which is assumed as circular.

Table 13.3 Thin limit of two-node beam. Modifications of transverse shear.

h	standard		RBF correction		shear scaling, eq. (13.29)	
n	w	θ	w	θ	w	θ
0	4.0002E+00	6.0000E–02	4.0003E+00	6.0000E–02	3.9999E+00	6.0000E–02
–1	3.9999E+03	6.0000E+01	4.0000E+03	6.0000E+01	3.9999E+03	6.0000E+01
–2	3.9999E+06	6.0000E+04	4.0000E+06	6.0000E+04	3.9999E+06	6.0000E+04
–3	4.0003E+09	6.0006E+07	4.0000E+09	6.0000E+07	3.9999E+09	6.0000E+07
–4	4.0239E+12	6.0230E+10	4.0000E+12	6.0000E+10	3.9999E+12	6.0000E+10
–5	2.1911E+14	6.7033E+12	4.2253E+15	6.3521E+13	4.2259E+15	6.3531E+13
–6	1.8068E+16	1.2498E+15	4.0000E+18	6.0000E+16	3.9999E+18	6.0000E+16
–7	2.2518E+17	5.4043E+16	4.0000E+21	6.0000E+19	3.9999E+21	6.0000E+19
–8	–6.9175E+18	-9.2234E+18	4.0000E+24	6.0000E+22	3.9999E+24	6.0000E+22

Consider a 2D circular arch 1-3-2 bent by two opposite horizontal forces P, see Fig. 13.10a. If a straight (not curved) two-node element linking nodes 1 and 2 is used, then the forces P do not cause bending in this element, which is incorrect, comparing to the arch. This can be corrected, e.g., by the method of *rigid links*, which introduces two rigid links 1-A and 2-B, and shifts the straight two-node element to the position defined by points A and B. Then, the forces P cause bending in this element, similarly as in the arch.

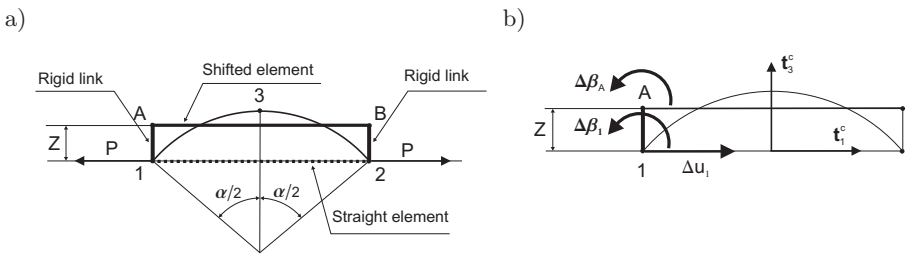

Fig. 13.10 Curvature correction for arch. a) Straight element and rigid links. b) Transformation for rotation.

The displacements and rotation for node A are defined as

$$\Delta u_A = \Delta u_1, \qquad \Delta w_A = \Delta w_1, \qquad \Delta\beta_A = \Delta\beta_1 + Z\,\Delta u_1, \qquad (13.38)$$

where only the rotation at node A is corrected and it depends on the rotation at node 1, the horizontal displacement Δu_1 at node 1, and the offset Z, see Fig. 13.10b.

The offset Z corresponds to the length of the rigid links. Its magnitude is arbitrary and must be somehow selected. We have tested two values:

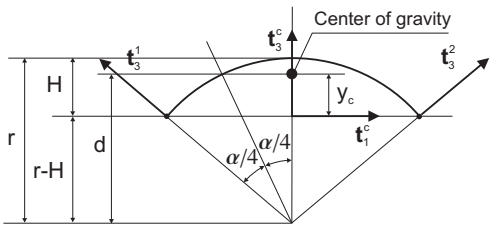

Fig. 13.11 Curvature correction. Center of gravity of arch.

- $Z = H$, where H is the height of arch, see Fig. 13.11, and
- $Z = y_c$, where y_c is the vertical coordinate of the center of gravity of an arch of a constant thickness in the local frame $\{\mathbf{t}_1^c, \mathbf{t}_3^c\}$,

$$y_c = d - (r - H), \qquad d = r\cos(\alpha/4), \tag{13.39}$$

where $\alpha = \alpha_1 + \alpha_2 = \arccos(\mathbf{t}_3^1 \cdot \mathbf{t}_3^c) + \arccos(\mathbf{t}_3^2 \cdot \mathbf{t}_3^c)$. This definition of α involves normal vectors at nodes 1, 2, and at the center, and can also be applied to shapes which are not exactly circular.

Note that the curvature correction must be performed in the local orthonormal basis at the element's center $\{\mathbf{t}_k^c\}$. Besides, the curvature correction slightly impairs a convergence rate of the Newton method, comparing to that for the uncorrected element, but accuracy is improved.

Numerical example. The circular arch is shown in Fig. 13.12. The left boundary is fixed, while at the right one, the horizontal force P is applied and the vertical displacement is constrained to zero. The RBF correction and the curvature correction are tested, using the two-node finite-rotation Timoshenko beam element with one-point integration.

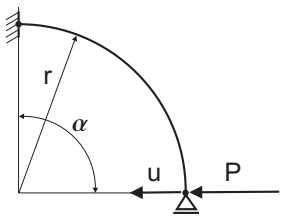

Fig. 13.12 Circular arch. $E = 3 \times 10^6$, $\nu = 0.3$, $r = 300$, $\alpha = 90^o$, $h = 3$.

The mesh convergence in a linear test is shown in Fig. 13.13a, where the normalizing reference value of the horizontal displacement is 3.3422.

a)

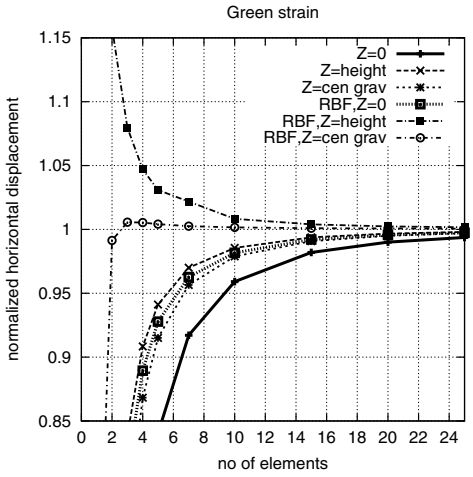

b)

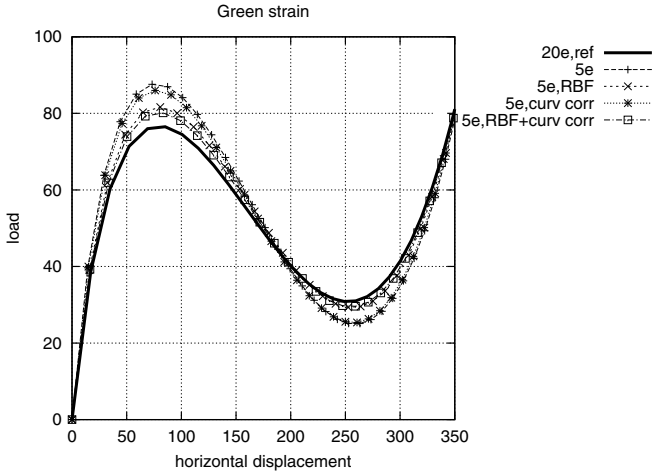

c)

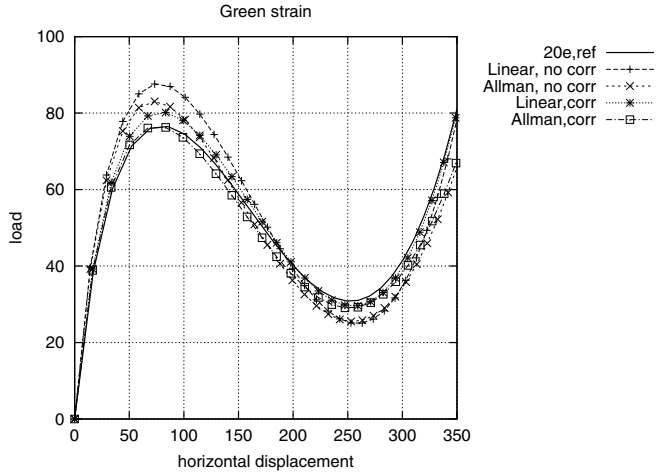

Fig. 13.13 Circular arch. Effect of the RBF and curvature corrections.
a) Linear test: mesh convergence. b) Nonlinear test.
c) Comparison of two elements "Linear" and "Allman" with/without corrections.

The best accuracy is obtained for both corrections combined together and when the offset $Z = y_c$. For the one-element mesh, the obtained result is not as exact as it was for a straight cantilever, but still the improvement is impressive; one corrected element provides an accuracy comparable with that for 25 uncorrected elements.

The results of a nonlinear test are shown for 5- and 20-element meshes in Fig. 13.13b. The offset $Z = y_c$ is used and its values are as follows: for 20 elements $Z = 0.17346 \approx 0.06h$, while for five elements $Z = 2.7687 \approx 0.92h$, i.e. is of the order of the thickness. The load increment is $\Delta P = 10$.

For five elements, the RBF correction has a stronger effect than the curvature correction but both corrections combined together produce the best result. The RBF correction itself halves the difference between the solutions for 20 and five elements without the RBF. The solution for 20 elements is used for reference, as then the effect of both corrections is negligible.

Finally, we compare the two earlier presented finite-rotation two-node Timoshenko elements, "Linear" and "Allman", the eigenvalues of which are given in Table 13.1. The mesh of five elements is used and solutions are obtained for two cases: (1) no corrections, and (2) with both corrections applied. The reference solution is obtained for a 20-element mesh, and is identical for both elements. Comparing the curves in Fig. 13.13c, we see that the "Allman" element performs better than the "Linear" element, and that the corrections improve the accuracy of both.

13.2 Treatment of transverse shear stiffness of shells

The problems caused by the transverse shear strains, such as the transverse shear locking and a poor performance of very thin elements, also appear for shells, for which we can generalize the techniques developed and tested for beams in Sect. 13.1.

Transverse shear strain for shell. For the Reissner kinematics, the transverse shear strain components in the ortho-normal basis $\{\mathbf{t}_\alpha\}$ are

$$\varepsilon_{\alpha 3} = \varepsilon_{3\alpha} = \tfrac{1}{2}\mathbf{x}_{0,\alpha} \cdot \mathbf{a}_3, \tag{13.40}$$

where the differentiation is performed w.r.t. S^α. The above form of the transverse shear strains is identical for the Green strain and the symmetric right stretch strain.

13.2.1 Selective Reduced Integration

The first remedy which was invented to circumvent the transverse shear locking (TSL) in a four-node plate element was the Selective Reduced Integration (SRI) proposed in [103]. The bending energy was integrated using the 2×2-point Gauss scheme, while the transverse shear energy was integrated by the reduced one-point scheme. Note that the plate element has only three dofs/node, i.e. the normal displacement w, and two tangent rotations θ_α.

However, differently from two-node Timoshenko beams, the under-integration of the transverse shear energy of a plate yields two spurious zero eigenvalues. The associated zero-energy modes are as follows: (i) the hourglass mode $w = \xi\eta$ and $\theta_\alpha = 0$, and (ii) the in-plane twisting mode $\theta_1 = -\eta$, $\theta_2 = \xi$ and $w = 0$, see [103], Fig. 10. According to this paper, the first mode can be removed by 2×2 integration of the $(\partial w/\partial x_\alpha)^2$ term in the transverse shear energy, while the second mode vanishes for a mesh with the rigid body modes removed.

Note that two schemes of integration of the transverse shear strain energy make the SRI complicated and inconvenient for materially nonlinear problems. This provided the motivation for further work, resulting in the ANS technique described in the next section.

For four-node shell elements, the under-integration of the transverse shear energy causes rank deficiency (two spurious zero eigenvalues), similarly as for plate elements, and, for this reason, is not currently used.

13.2.2 Assumed Natural Strain method

Overview. In the Assumed Natural Strain (ANS) method each strain component is treated separately; it is sampled at selected points and approximated over the element domain.

For example, the transverse shear strain $\varepsilon_{13}(\xi, \eta)$ is sampled at two points $(\xi = 0, \eta = \pm 1)$ and approximated by a function which is constant in the ξ-direction and linear in the η-direction. This means that in unidirectional bending in the $\xi\zeta$-plane, the rectangular four-node shell element performs identically as the two-node beam element.

The constant approximation in the ξ-direction corresponds to the reduced one-point integration in the ξ-direction but, when we use the ANS method, we can apply the standard 2×2-point Gauss integration to all terms, including the transverse shear strain energy.

The ANS method was gradually developed in several works, including [138, 104, 139, 18, 19]. The works preceding [18] are well characterized in [141], pp. 401–3. The controversy existed over the optimal position of points in the direction in which the strain is linearly approximated and two values were in use: $\pm 1/\sqrt{3}$ and ± 1. Currently, the latter one is considered as better.

Note that the assumed strain method is also used in nine-node shell elements for which more sophisticated sampling and approximation schemes are used to eliminate the transverse shear and membrane locking, see Sect. 14.4.

Covariant components of transverse shear strains. In eq. (13.40), for the transverse shear strain, the differentiation is performed w.r.t. S^α, but the position vector $\mathbf{x}_0$ is approximated in terms of the natural coordinates $\xi, \eta \in [-1, +1]$. Hence, we have to express the derivatives w.r.t. S^α by the derivatives w.r.t. ξ, η.

Let us form the vector of components of the transverse shear strain of eq. (13.40),

$$\begin{bmatrix} \varepsilon_{13} \\ \varepsilon_{23} \end{bmatrix} = \begin{bmatrix} \frac{1}{2}\mathbf{x}_{0,1} \cdot \mathbf{a}_3 \\ \frac{1}{2}\mathbf{x}_{0,2} \cdot \mathbf{a}_3 \end{bmatrix}, \tag{13.41}$$

where the differentiation is performed w.r.t. S^α and the position vector $\mathbf{x}_0$ is approximated as $\mathbf{x}_0(\xi, \eta) = \sum_{I=1}^4 N_I(\xi, \eta)\, \mathbf{x}_{0I}$. Then we transform

$$\begin{bmatrix} \frac{1}{2}\mathbf{x}_{0,1} \cdot \mathbf{a}_3 \\ \frac{1}{2}\mathbf{x}_{0,2} \cdot \mathbf{a}_3 \end{bmatrix} = \sum_{I=1}^4 \begin{bmatrix} \frac{1}{2}N_{I,1}\, \mathbf{x}_{0I} \cdot \mathbf{a}_3 \\ \frac{1}{2}N_{I,2}\, \mathbf{x}_{0I} \cdot \mathbf{a}_3 \end{bmatrix} = \sum_{I=1}^4 \begin{bmatrix} N_{I,1} \\ N_{I,2} \end{bmatrix} s_I \tag{13.42}$$

where the auxiliary scalar $s_I \doteq \frac{1}{2}\mathbf{x}_{0I} \cdot \mathbf{a}_3$. To calculate the derivatives of shape functions, we can use eq. (2.46),

$$\begin{bmatrix} N_{I,1} \\ N_{I,2} \end{bmatrix} = \mathbf{J}^{-T} \begin{bmatrix} N_{I,\xi} \\ N_{I,\eta} \end{bmatrix}, \tag{13.43}$$

with the Jacobian inverse $\mathbf{J}^{-1}$ defined by eq. (10.56). Then

$$\sum_{I=1}^4 \begin{bmatrix} N_{I,1} \\ N_{I,2} \end{bmatrix} s_I = \mathbf{J}^{-T} \sum_{I=1}^4 \begin{bmatrix} N_{I,\xi} \\ N_{I,\eta} \end{bmatrix} s_I = \mathbf{J}^{-T} \begin{bmatrix} \frac{1}{2}\mathbf{x}_{0,\xi} \cdot \mathbf{a}_3 \\ \frac{1}{2}\mathbf{x}_{0,\eta} \cdot \mathbf{a}_3 \end{bmatrix}, \tag{13.44}$$

and the differentiation is performed w.r.t. ξ, η. Hence, eq. (13.41) can be rewritten as

$$\begin{bmatrix} \varepsilon_{13} \\ \varepsilon_{23} \end{bmatrix} = \mathbf{J}^{-T} \begin{bmatrix} \varepsilon^{\xi}_{13} \\ \varepsilon^{\xi}_{23} \end{bmatrix}, \tag{13.45}$$

where

$$\varepsilon^{\xi}_{13} \doteq \tfrac{1}{2}\mathbf{x}_{0,\xi} \cdot \mathbf{a}_3, \qquad \varepsilon^{\xi}_{23} \doteq \tfrac{1}{2}\mathbf{x}_{0,\eta} \cdot \mathbf{a}_3. \tag{13.46}$$

Note that eq. (13.45) transforms the covariant ($\alpha 3$) components of a tensor into Cartesian components, similarly as in eq. (2.27). The covariant components $\varepsilon^{\xi}_{\alpha 3}$ are interpolated within the ANS method in a specific way which is described below.

The ANS method. The Assumed Natural Strain (ANS) method consists of the following steps:

1. The covariant components $\varepsilon^{\xi}_{\alpha 3}$ of eq. (13.46) are evaluated (sampled) at the mid-side points of element edges, at two points for each component, see Fig. 13.14. The sampled values are denoted as $\varepsilon^{M}_{\alpha 3}$, $M = 5, 6, 7, 8$.

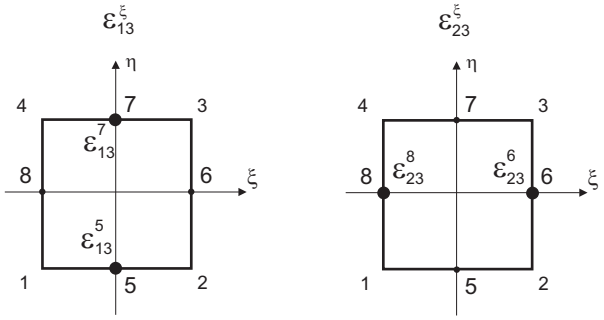

Fig. 13.14 Location of sampling points to evaluate ε^{ξ}_{13} and ε^{ξ}_{23}.

2. The components $\varepsilon^{\xi}_{\alpha 3}$ are approximated over the element domain as follows:

$$\varepsilon^{\xi}_{13}(\xi,\eta) = \tfrac{1}{2}\left[(1-\eta)\,\varepsilon^{5}_{13} + (1+\eta)\,\varepsilon^{7}_{13}\right], \tag{13.47}$$

$$\varepsilon^{\xi}_{23}(\xi,\eta) = \tfrac{1}{2}\left[(1-\xi)\,\varepsilon^{6}_{23} + (1+\xi)\,\varepsilon^{8}_{23}\right], \tag{13.48}$$

where the sampled values $\varepsilon^{M}_{\alpha 3}$ are used. These approximations are constant in the direction in which the derivative is calculated in eq. (13.46) and linear in the other direction, which means that the ANS method is orientation-dependent.

3. At the Gauss integration points, the transverse shear strain $\varepsilon_{\alpha 3}$ is evaluated by eq. (13.45),

$$\begin{bmatrix} \varepsilon_{13} \\ \varepsilon_{23} \end{bmatrix} = \mathbf{J}_{Lc}^{-T} \begin{bmatrix} \varepsilon_{13}^{\xi} \\ \varepsilon_{23}^{\xi} \end{bmatrix}, \tag{13.49}$$

where the Jacobian is local (L) and evaluated at the element center (c). Note that the Jacobian is not approximated by the ANS method ! We have also tested the version with the Jacobian matrix not taken at the center but at the Gauss Points, i.e. using $\mathbf{J}_L$ not $\mathbf{J}_{Lc}$. It also passes the bending patch test and the difference of both solutions in other tests is negligible.

The ANS method effectively removes the transverse shear locking and is used in four-node shell elements as a standard.

Test 1. Unidirectional bending in $\xi\zeta$-plane. Consider a 1×1 square element shown in Fig. 13.15. Nodes 1 and 4 are fixed, while at nodes 2 and 3 we apply: (i) the displacement vector $\mathbf{u} = [0, 0, 0.1]^T$, and (ii) the rotation vector $\boldsymbol{\psi} = [0,\, 0.01,\, 0.01]^T$. The rotations are small so the forward-rotated normal vector can be computed as $\mathbf{a}_3 = \mathbf{t}_3 + \boldsymbol{\psi} \times \mathbf{t}_3$.

The transverse shear ε_{23}^{ξ} is equal to zero, while the distribution of ε_{13}^{ξ} obtained for bilinear approximations is shown in Fig. 13.15. In the ANS method, ε_{13}^{ξ} is sampled at points 5 and 7, and approximated by eq. (13.47). Hence, for the unidirectional bending in the $\xi\zeta$-plane, we obtain $\varepsilon_{13}^{\xi}(\xi, \eta)$ which is constant in both directions!

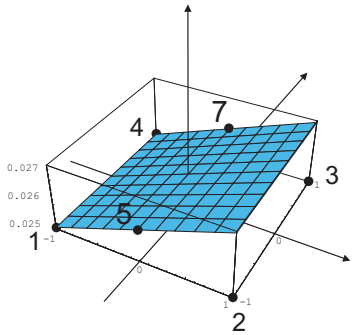

Fig. 13.15 Transverse shear ε_{13}^{ξ} for unidirectional bending.

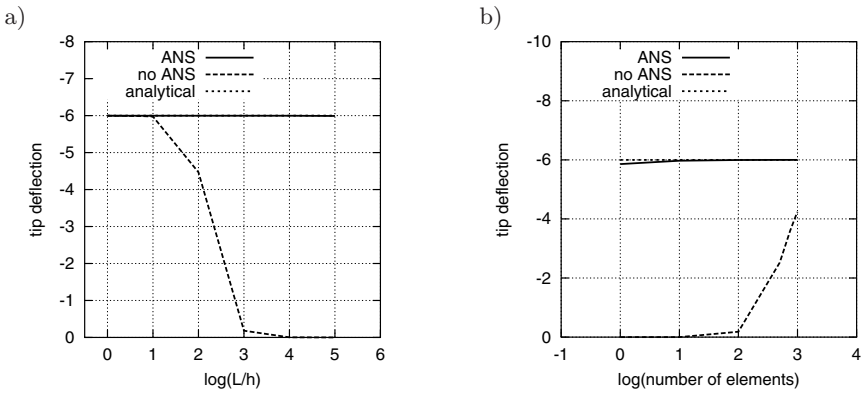

Fig. 13.16 Tip deflection for pure bending. a) Thin limit. b) Mesh convergence.

Test 2. Pure bending of slender cantilever. In this example, we compare results obtained by the same shell element either with or without the ANS procedure.

The data for the cantilever is defined in Sect. 15.3.1 and the cantilever is shown in Fig. 15.13. The mesh of $m \times 1$ four-node shell elements is used.

The bending moment $M = 0.1$ is applied, for which the analytical displacement at the cantilever's tip is $w = ML^2/(2EI) = -6$, where $I = bh^3/12$. Two numerical tests were performed using the four-node shell element:

1. Test of thin limit, in which thickness h was changed, see Fig. 13.16a. 100 elements were used and the moment M was scaled by h^3, to make results independent of thickness. When the ANS procedure is not applied, then the response is too stiff, due to the TSL.
2. Test of mesh convergence with the number of elements m changed. The results are shown in Fig. 13.16b. We see slow convergence when the ANS procedure is not applied, caused by the TSL.

13.2.3 RBF correction for shells

The motivation for using the RBF correction to four-node shell elements is analogous as for two-node beam elements, see Sect. 13.1.2. Note that for the shell element, we can have a two-directional sinusoidal bending, see Fig. 13.17, which can be rendered by bending moments applied to nodes.

The way in which the RBF correction can be applied to four-node shell elements is described in [138], p. 178 and some additional suggestions are

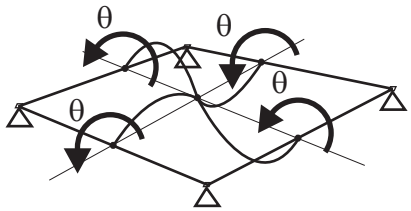

Fig. 13.17 Sinusoidal bending of four-node shell element.

given in [140], p. 104. Usefulness of the RBF correction for higher-order hierarchical p elements is acknowledged in [142], p. 184.

In our implementation of the RBF correction for a four-node bilinear element and an isotropic elastic SVK material, we use the corrected shear modulus G^* of eq. (13.16) separately for each direction, i.e.

$$G_1^* = \left(\frac{1}{G} + \frac{l_1^2}{h^2 E}\right)^{-1}, \qquad G_2^* = \left(\frac{1}{G} + \frac{l_2^2}{h^2 E}\right)^{-1}, \tag{13.50}$$

where l_1 and l_2 are the lengths of vectors connecting opposite mid-side points. The most straightforward implementation is to express the transverse shear strain energy for a single element as follows:

$$\mathcal{W}_\gamma = 2h \int_{-1}^{+1} \int_{-1}^{+1} \left(G_1^*\, \varepsilon_{13}^2 + G_2^*\, \varepsilon_{23}^2\right)\, J \,\mathrm{d}\xi \mathrm{d}\eta, \tag{13.51}$$

where h, G_1^*, and G_2^* are constant over the element. Then the element passes the bending patch test and performs well for bending but, unfortunately, yields erroneous results for twist. This can be observed, e.g., in the linear test of a slender cantilever modelled by one layer of four-node elements, see Sect. 15.3.1. For $h = 0.01$ and twisting by a pair of end forces, the rotation r_x of the tip is too large by about 38%, see the example in the sequel. That is why a more sophisticated approach is needed.

To avoid an excessive twist, it was proposed in [140], p. 104 to apply the full RBF correction to the average values of the (sampled) transverse shear strains, while 4% of the correction to the remaining parts of them. This idea is reconsidered below.

Note that the RBF correction is implemented on top of the ANS method which we use for the transverse shear strain, see Sect. 13.2.2. (Note that the version of the ANS method which we use is different from

that used in [138].) The approximations (13.47) and (13.48) of the ANS method can be rewritten as follows

$$\varepsilon_{13}^{\xi}(\xi,\eta) = \tfrac{1}{2}\left(\varepsilon_{13}^{5} + \varepsilon_{13}^{7}\right) + \eta\ \tfrac{1}{2}\left(\varepsilon_{13}^{7} - \varepsilon_{13}^{5}\right) = \varepsilon_{13}^{\mathrm{ave}} + \eta\,\varepsilon_{13}^{\mathrm{d}}, \tag{13.52}$$

$$\varepsilon_{23}^{\xi}(\xi,\eta) = \tfrac{1}{2}\left(\varepsilon_{23}^{6} + \varepsilon_{23}^{8}\right) + \xi\ \tfrac{1}{2}\left(\varepsilon_{23}^{8} - \varepsilon_{23}^{6}\right) = \varepsilon_{23}^{\mathrm{ave}} + \xi\,\varepsilon_{23}^{\mathrm{d}}, \tag{13.53}$$

where, in the final forms, we distinguish the average values "ave" and the differences "d" of the sampled strain components. Then the transverse shear strains of eq. (13.49) are

$$\begin{bmatrix} \varepsilon_{13} \\ \varepsilon_{23} \end{bmatrix} = \mathbf{J}_{Lc}^{-T} \begin{bmatrix} \varepsilon_{13}^{\mathrm{ave}} + \eta\,\varepsilon_{13}^{\mathrm{d}} \\ \varepsilon_{23}^{\mathrm{ave}} + \xi\,\varepsilon_{23}^{\mathrm{d}} \end{bmatrix}, \tag{13.54}$$

where

$$\mathbf{J}_{Lc}^{-1} = \begin{bmatrix} \bar{J}_{11} & \bar{J}_{12} \\ \bar{J}_{21} & \bar{J}_{22} \end{bmatrix} \tag{13.55}$$

is evaluated at the element center i.e. is constant in ξ and η. Hence, the 13-component is a linear function of ξ and η,

$$\begin{aligned} \varepsilon_{13} &= (\bar{J}_{11}\varepsilon_{13}^{\mathrm{ave}} + \bar{J}_{21}\varepsilon_{23}^{\mathrm{ave}}) + \bar{J}_{21}\varepsilon_{33}^{\mathrm{d}}\,\xi + \bar{J}_{11}\varepsilon_{13}^{\mathrm{d}}\,\eta \\ &= \bar{\varepsilon}_{13}^{\mathrm{ave}} + \bar{\varepsilon}_{13}^{\mathrm{d1}}\,\xi + \bar{\varepsilon}_{13}^{\mathrm{d2}}\,\eta, \end{aligned} \tag{13.56}$$

where the parts "ave" and "d" are separated and "d" is additionally split into parts "d1" and "d2" multiplied by ξ and η respectively. The definitions of the $\bar{\varepsilon}_{\alpha 3}$ terms are obvious. As we shall see below, separation of these parts in the strain energy requires additional simplifications.

The Jacobian determinant for a four-node bilinear element is $J(\xi,\eta) = J_0 + J_1\xi + J_2\eta$, see eq. (10.63). Both ε_{13} and J are linear functions of ξ and η and the integration yields

$$\begin{aligned} &\int_{-1}^{+1}\int_{-1}^{+1} \varepsilon_{13}^{2}\ J\,\mathrm{d}\xi\mathrm{d}\eta = \\ &\quad 4(\bar{\varepsilon}_{13}^{\mathrm{ave}})^2 J_0 + \frac{4}{3}\left[(\bar{\varepsilon}_{13}^{\mathrm{d1}})^2 + (\bar{\varepsilon}_{13}^{\mathrm{d2}})^2\right] J_0 + \frac{8}{3}\left[\bar{\varepsilon}_{13}^{\mathrm{ave}}(\bar{\varepsilon}_{13}^{\mathrm{d1}} J_1 + \bar{\varepsilon}_{13}^{\mathrm{d2}} J_2)\right], \end{aligned} \tag{13.57}$$

where the "ave" and "d" terms in the last bracket are coupled. Two ways of treating of this coupling can be used.

1. The first way is in the spirit of the suggestion of [140], p. 104. The separation of the "ave" and "d" terms can be achieved by using a simplified form of ε_{13}^2,

$$\varepsilon_{13}^2 \approx (\bar{\varepsilon}_{13}^{\mathrm{ave}})^2 + (\bar{\varepsilon}_{13}^{\mathrm{d1}})^2\,\xi^2 + (\bar{\varepsilon}_{13}^{\mathrm{d2}})^2\,\eta^2, \tag{13.58}$$

obtained by omitting the linear terms. The bilinear term is also omitted as it yields zero in integration. For the simplified ε_{13}^2,

$$\int_{-1}^{+1}\int_{-1}^{+1} \varepsilon_{13}^2\; J\,\mathrm{d}\xi\mathrm{d}\eta \approx \frac{4}{3}\left[3(\bar{\varepsilon}_{13}^{\mathrm{ave}})^2 + (\bar{\varepsilon}_{13}^{\mathrm{d1}})^2 + (\bar{\varepsilon}_{13}^{\mathrm{d2}})^2\right] J_0, \tag{13.59}$$

in which the terms "ave" and "d" of the sampled strains are separated. (Note that the same result of integration is obtained for the full form of ε_{13}^2 and $J(\xi,\eta) \approx J_0$.) Finally, the integrand of the strain energy (13.51) is modified as follows:

$$G_1^*\,\varepsilon_{13}^2 \approx G_1^*\,(\bar{\varepsilon}_{13}^{\mathrm{ave}})^2 + G_{1c}^*\,(\bar{\varepsilon}_{13}^{\mathrm{d1}})^2\,\xi^2 + G_{1c}^*\,(\bar{\varepsilon}_{13}^{\mathrm{d2}})^2\,\eta^2, \tag{13.60}$$

where the additionally corrected shear modulus is defined as

$$G_{1c}^* \doteq \left(\frac{1}{G} + a\,\frac{l_1^2}{h^2 E}\right)^{-1}, \qquad a \doteq \frac{c}{c + (1-c)\,(l_1/l_2)^2}, \tag{13.61}$$

where c is a corrective coefficient, designated as ϵ in [138]. Besides, (l_1/l_2) is the element aspect ratio, as the average size of an element in each direction is $l_1 \doteq \frac{1}{2}(-x_1 + x_2 + x_3 - x_4)$ and $l_2 \doteq \frac{1}{2}(-y_1 - y_2 + y_3 + y_4)$, where x_I and y_I are coordinates of nodes $I = 1,2,3,4$ in the local Cartesian basis at the element's center, $\{\mathbf{t}_k^c\}$. Too small values of c can cause problems with the conditioning of the stiffness matrix; the value 0.04 is selected in [138].

Similar expressions can be obtained for ε_{23},

$$G_2^*\,\varepsilon_{23}^2 \approx G_2^*\,(\bar{\varepsilon}_{23}^{\mathrm{ave}})^2 + G_{2c}^*\,(\bar{\varepsilon}_{23}^{\mathrm{d1}})^2\,\xi^2 + G_{2c}^*\,(\bar{\varepsilon}_{23}^{\mathrm{d2}})^2\,\eta^2, \tag{13.62}$$

where the additionally corrected shear modulus is defined as

$$G_{2c}^* \doteq \left(\frac{1}{G} + b\,\frac{l_2^2}{h^2 E}\right)^{-1}, \qquad b \doteq \frac{c}{c + (1-c)\,(l_2/l_1)^2}. \tag{13.63}$$

2. In our treatment of the coupling, the full RBF correction is applied to the average values but a fraction of it is applied to the whole remaining

part, not to the differences of the transverse shear strains, as in the previous method. Then we modify the integrand of the strain energy (13.51) as follows:

$$G_1^* \, \varepsilon_{13}^2 \approx G_1^* \, (\bar{\varepsilon}_{13}^{\mathrm{ave}})^2 + G_{1c}^* \, \left[\varepsilon_{13}^2 - (\bar{\varepsilon}_{13}^{\mathrm{ave}})^2 \right], \tag{13.64}$$

$$G_2^* \, \varepsilon_{23}^2 \approx G_2^* \, (\bar{\varepsilon}_{23}^{\mathrm{ave}})^2 + G_{2c}^* \, \left[\varepsilon_{23}^2 - (\bar{\varepsilon}_{23}^{\mathrm{ave}})^2 \right], \tag{13.65}$$

where G_{1c}^* and G_{2c}^* are defined in eqs. (13.61) and (13.63).

This formula was implemented for shell elements based on the potential energy; the modifications necessary for the mixed functionals are described below. This method works very well as we can see in the example presented in the sequel.

RBF correction for mixed formulations of shells. For the Hellinger–Reissner functional and the Hu–Washizu functional, the modifications related to the RBF correction are as follows:

Hellinger–Reissner functional. Normally, the stress corresponding to the assumed strain is calculated as $\sigma_{13}^a = 2G \, \varepsilon_{13}^a$, while with the RBF correction, we compute

$$\sigma_{\alpha 3}^a = 2G_\alpha^* \, (\bar{\varepsilon}_{\alpha 3}^a)^{\mathrm{ave}} + 2G_{\alpha c}^* \, [\varepsilon_{\alpha 3}^a - (\bar{\varepsilon}_{\alpha 3}^a)^{\mathrm{ave}}], \qquad \alpha = 1, 2, \tag{13.66}$$

where $(\bar{\varepsilon}_{\alpha 3}^a)^{\mathrm{ave}}$ is the average value of the assumed strain.

Hu–Washizu functional. The strain energy corresponding to the assumed strain is calculated as in eq. (13.65), i.e.

$$\mathcal{W}(\varepsilon_{\alpha 3}^a) = G_\alpha^* \, [(\bar{\varepsilon}_{\alpha 3}^a)^{\mathrm{ave}}]^2 + G_{\alpha c}^* \left\{ (\varepsilon_{\alpha 3}^a)^2 - [(\bar{\varepsilon}_{\alpha 3}^a)^{\mathrm{ave}}]^2 \right\}, \quad \alpha = 1, 2, \tag{13.67}$$

while the other parts are not modified.

Linear example: Twisted cantilever. Consider the slender initially flat cantilever of Sect. 15.3.1, see Fig. 15.13, twisted by a pair of vertical transverse forces $P_z = \pm 1$. One layer of four-node shell elements is used and the shell thickness, $h = 0.01$.

The displacements and rotations at the tip node obtained by a linear analysis are presented in Table 13.4. Comparing the results obtained without the RBF correction for the 100×1-element mesh and the 100×9-element mesh, we see that the RBF correction is not needed for the twist.

Because we use the RBF correction to improve the sinusoidal bending, we have to select such a value of c for which the results of twist are unaffected. The value $c = 0$ yields almost exact results, but, unfortunately, then the problem with conditioning of the stiffness matrix appears. This problem disappears for $c = 0.01$; a slightly higher value $c = 0.04$ is suggested in [138].

For reference, we use the solution obtained by the shell element with six dofs/node of FEAP, described in [235]. This is the Discrete Kirchhoff Quadrilateral (DKQ) element, with linear kinematics (small strains and rotations), based on the Allman shape functions and with the bending part of [20].

Table 13.4 Effect of the RBF correction for characteristic values of c. Twist of slender cantilever by forces $P_z = \pm 1$. Shell element EADG4-PL-Warped.

Mesh	RBF correction	Displacement $u_z/10^2$	Rotations $r_x/10^2$	r_y
100×1	no	3.8897	7.7788	-3.9001
100×9	no	3.8922	7.7828	-3.8987
100×1	yes, c=0 (*)	3.8896	7.7787	-3.9001
	yes, c=0.005 (*)	3.8973	7.7933	-3.8995
	yes, c=0.01	3.9050	7.8082	-3.8986
	yes, c=0.04	3.9508	7.8980	-3.8899
	yes, c=0.1	4.0419	8.0784	-3.8633
100×1, FEAP		3.8929	7.785	-3.9000

(*) Conditioning problem: D-max/D-min $\approx 10^{10}$

13.2.4 Miscellaneous topics

EAS method for transverse shear strains. Recall that eq. (13.45) specifies a transformation of the covariant transverse shear strains to the local orthonormal basis

$$\begin{bmatrix} \varepsilon_{13} \\ \varepsilon_{23} \end{bmatrix} = \mathbf{J}^{-T} \begin{bmatrix} \varepsilon^{\xi}_{13} \\ \varepsilon^{\xi}_{23} \end{bmatrix}. \tag{13.68}$$

Within the EAS method, we can assume the following representation for the enhanced transverse shear components

$$\begin{bmatrix} \varepsilon^{\text{enh}}_{13} \\ \varepsilon^{\text{enh}}_{23} \end{bmatrix} = \mathbf{J}_c^{-T} \begin{bmatrix} \xi\, q_1 + \xi\eta\, q_2 \\ \eta\, q_3 + \xi\eta\, q_4 \end{bmatrix} \left(\frac{j_c}{j} \right). \tag{13.69}$$

Such a representation was used in [201], eqs. (97) and (98). The role of (j_c/j) is identical to that for the membrane enhancement. The enhancement is added to the compatible part of the transverse shear strains treated by the ANS method.

Discrete Kirchhoff (DK) elements. If the transverse shear is negligible, then we can exploit this fact using the Kirchhoff constraint, $\varepsilon_{\alpha 3} = 0$, at selected discrete points to modify the shape functions. This leads to the so-called Discrete Kirchhoff (DK) family of elements; beams, plates, and shells. This concept is considered in [246, 247].

1. The two-node Discrete Kirchhoff Beam (DKB) is based on a cubic approximation of normal displacement w, see eq. (13.18), and a quadratic approximation of rotation θ. First, the Hermitian-type shape functions are obtained for w which are expressed by values of w and $w_{,\xi}$ at nodes and, next, two DK constraints are applied at these nodes, which yields eq. (13.21). Additionally, one DK constraint is applied at the element center to accommodate the quadratic term of the rotation.
2. The four-node Discrete Kirchhoff Quadrilateral (DKQ) for plates was proposed in [20]. The approach to plates is a natural extension of the concept for the DK beam and was used as the bending part of several shell elements in [117, 113, 235].
3. Several Discrete Kirchhoff Triangle (DKT) plate and shell elements can also be found in the literature.

The DK elements are based on polynomials of relatively high order and perform very well in bending, including sinusoidal bending, and twisting. However, they neglect the transverse shear energy and can be used only for thin shells.

Kirchhoff limit for transverse shear constrained to zero. The formulation based on the Reissner hypothesis can be constrained by enforcing the RC $\text{skew}(\mathbf{Q}^T\mathbf{F}) = \mathbf{0}$ for the $\alpha 3$ components only, which means that the transverse shear strain $\varepsilon_{\alpha 3} = 0$.

As an example, we analyze the cantilever shown in Fig. 15.13; the data is defined in Sect. 15.3.1, but the thickness $h = 10^n$, where $n \in [-3, +3]$. The mesh consists of 100 two-node Timoshenko beam elements. The 13-component of $\text{skew}(\mathbf{Q}^T\mathbf{F}) = \mathbf{0}$ is enforced using the penalty method with $\gamma = 2G\,h \times 10^3$.

The original and constrained Reissner solutions are shown in Table 13.5. The tip displacement w is affected by the constraint and indeed forced to attain the Kirchhoff limit 4×10^{-3n} for $h > 10^{-1}$. Note that w of the original element is bigger than w of the constrained element!

The tip rotation θ is in accordance with the Kirchhoff solution $6 \times 10^{-2-3n}$ for the whole range of h, except for the very thin beam of $h = 10^{-3}$, for which the solution is destroyed by the penalty method.

Table 13.5 Effect of 13-component of $\text{skew}(\mathbf{Q}^T\mathbf{F}) = \mathbf{0}$ on Timoshenko beam.

Thickness n	Solution type	Displacement w	Rotation θ
+3	original	3.1600E–07	6.0000E–11
	constrained	4.1298E–09	6.0000E–11
+2	original	7.1199E–06	6.0000E–08
	constrained	4.0012E–06	6.0000E–08
+1	original	4.0311E–03	6.0000E–05
	constrained	3.9999E–03	6.0000E–05
0	original	4.0002E+00	6.0000E–02
	constrained	3.9999E+00	6.0000E–02
–1	original	3.9999E+03	6.0000E+01
	constrained	3.9999E+03	6.0000E+01
–2	original	3.9999E+06	6.0000E+04
	constrained	4.0009E+06	6.0050E+04
–3	original	4.0003E+09	6.0006E+07
	constrained	5.3823E+08	1.1540E+07
	Kirchhoff limit	4×10^{-3n}	$6 \times 10^{-2-3n}$